

# Structure determination of the hexagonal quasicrystal approximant $\mu'$ -(Al,Si)<sub>4</sub>Cr by the strong reflections approach

Z.B. He<sup>a,b</sup>, X.D. Zou<sup>c,\*</sup>, S. Hovmöller<sup>c</sup>, P. Oleynikov<sup>c</sup>, K.H. Kuo<sup>a,b</sup>

<sup>a</sup>Department of Materials Technology, Dalian University of Technology, 116024 Dalian, China

<sup>b</sup>Beijing Laboratory of Electron Microscopy, Institute of Physics, Chinese Academy of Sciences, P.O. Box 603, 100080 Beijing, China

<sup>c</sup>Structural Chemistry, Stockholm University, SE-106 91 Stockholm, Sweden

Received 22 February 2006; accepted 13 March 2006

## Abstract

A number of different crystalline phases have been found in Al-rich Al–Cr–Si alloys by transmission electron microscopy (TEM). Among these, the new hexagonal phase  $\mu'$ -(Al,Si)<sub>4</sub>Cr ( $a = 2.01$  and  $c = 1.24$  nm) often found coexisting with the hexagonal  $\mu$ -(Al,Si)<sub>4</sub>Cr ( $a = 1.998$  and  $c = 2.4673$  nm, isostructural with  $\mu$ -Al<sub>4</sub>Mn) and also with the hexagonal  $\lambda$ -(Al,Si)<sub>4</sub>Cr ( $a = 2.839$  and  $c = 1.239$  nm, isostructural with  $\lambda$ -Al<sub>4</sub>Mn). It is evident from their electron diffraction patterns that the structures of these three phases are related. The strong reflections in all three are distributed in a similar way. They all exhibit a pseudo-icosahedral symmetry. The structure factor amplitudes and phases for the strong reflections of the  $\mu'$  phase could therefore be adopted from those of the  $\lambda$  phase, according to the strong reflections approach. A structure model of the  $\mu'$  phase is thus deduced from the known  $\lambda$ -Al<sub>4</sub>Mn.  $\mu'$  consists of chains of 3 + 3 or 4 + 2 interpenetrated icosahedra along the  $\langle 100 \rangle$  directions. Similar to the  $\lambda$  phase, there are two flat layers (F) and four puckered layers (P) in each unit cell of  $\mu'$ , stacked along the  $c$ -axis in a sequence of PFP(PFP)' where the (PFP)' block is related to the PFP block by a  $6_3$  screw.

© 2006 Elsevier B.V. All rights reserved.

**Keywords:** Aluminum-based quasicrystals; Hexagonal phases; Structural model; Icosahedral chains

## 1. Introduction

Since the discovery of the icosahedral quasicrystal in rapidly solidified Al–Mn alloys [1], the structures of quasicrystals have been one of the most interesting subjects in crystallography. Although there is no more problem to get stable quasicrystals, it is still difficult to solve the structures of quasicrystals by single-crystal X-ray diffraction due to the presence of defects in quasicrystals. For electron microscopy (EM), very small crystals are sufficient. Thus EM has been one of the most important techniques for studying quasicrystals. Quasicrystals are sometimes found to coexist with some crystalline phases that are related to the quasicrystals: quasicrystal approximants. Quasicrystals and their approximants usually have

well-defined orientation relationships. The distributions of the strong reflections in reciprocal space are very similar in quasicrystals and their related approximants. Thus, the structures of quasicrystal approximants are also closely related to those of quasicrystals and determining the structures of approximants is a very important step towards the understanding of quasicrystal structures.

Most quasicrystal approximants were discovered by electron microscopy. The crystals are often too small for single-crystal X-ray diffraction. Electron crystallography is a powerful method for solving structures of these approximants. An advantage of electron crystallography over X-rays is that the phases of crystallographic structure factors can be obtained directly from high-resolution EM (HREM) images. The structure of a very complex quasicrystal approximant  $\nu$ -AlCrFe (space group  $P6_3/m$ ,  $a = 40.687$  and  $c = 12.546$  Å) was recently determined from HREM images and electron diffraction patterns

\*Corresponding author. Tel.: +46 8 16 23 80; fax: +46 8 16 31 18.

E-mail address: [zou@struc.su.se](mailto:zou@struc.su.se) (X.D. Zou).

from 13 different zone axes [2]. However, this method requires extensive experimental work and image processing.

An alternative way of deducing the structure of an unknown approximant is from the structure of a related, known approximant. We have developed a new approach, the strong reflections approach for this purpose. The strong reflections approach has been successfully applied to a series of approximants in the ZnMgRe [3] systems, and recently also to the  $\tau(\mu)$  phase in the Al–Cr–Si system [4]. The key of the strong reflections approach is that, for a series of closely related approximants, the structure factors of these approximants are similar when the origin of the unit cell is at the same position. This means that not only the intensity distribution of the strong reflections in reciprocal space is similar, but also the phases of the structure factors are the same for these approximants. In such cases, the large structure factors calculated from the coordinates of a known approximant can be used as approximate structure factors of the unknown approximant. A 3D electron density map calculated from only those large structure factors (strong reflections) will be a good approximation of the real electron density map of the unknown approximant. A detailed and accurate atomic structure can be deduced from this 3D electron density map.

In Al-rich Al–Si–Cr alloys, several quasicrystal approximants of the general formula  $(\text{Al,Si})_4\text{Cr}$  have been identified by selected-area electron diffraction (SAED) [5]. The SAED patterns of the hexagonal  $\mu$ - and  $\lambda$ - $(\text{Al,Si})_4\text{Cr}$  phases are almost identical to those of their counterparts in Al–Mn or Al–Cr alloys, namely, the  $\mu$ - $\text{Al}_4\text{Mn}$  [6] ( $\text{P6}_3/\text{mmc}$ ,  $a \cong 2.00$  nm and  $c \cong 2.47$  nm)/ $\mu$ - $\text{Al}_4\text{Cr}$  [7–10] and  $\lambda$ - $\text{Al}_4\text{Mn}$  phases ( $\text{P6}_3/\text{m}$ ,  $a = 2.8382$  and  $c = 1.2389$  nm) [11]. In addition, two new phases related to  $\mu$  have been found: the  $\mu'$  phase ( $\text{P6}_3/\text{mmc}$ ,  $a = 2.01$  nm and  $c = 1.24$  nm) [6] and the  $\tau(\mu)$  phase ( $\text{P6}_3/\text{mmc}$ ,  $a = 3.23$  nm and  $c = 1.24$  nm) with its  $a$  parameter being about  $\tau = (1 + \sqrt{5})/2 \cong 1.61803$  times greater than that of  $\mu$  [12]. The structural model of the layer structure of  $\tau(\mu)$  was derived by the strong reflections approach [4] using the phases of the strong reflections of  $\lambda$ . Here, we present an electron diffraction study of the  $\mu'$  phase and the deduction of its structure model using the strong reflections approach developed by Hovmöller, Zou and others [3,4,13].

## 2. Experimental procedures

Al-rich Al–Si–Cr alloys with 5–15 at% Si and 20–27 at% Cr were prepared by repeated melting of high-purity Al, Cr and Si in an arc furnace followed by quenching or further annealing at 800–900 °C for 20 h. TEM samples were prepared by slicing, mechanical thinning and subsequent Ar ion milling. Selected-area electron diffraction (SAED) patterns were taken on a Philips CM200-FEG TEM operated at 200 kV. The crystals of  $\mu'$ ,  $\mu$  and  $\lambda$  phases were tilted in the TEM and a series of SAED patterns

along different zone axes were collected. The composition of the  $\mu'$  phase was determined by energy dispersive X-ray spectroscopy (EDS) to be  $\text{Al}_{71.9}\text{Si}_{8.1}\text{Cr}_{20.0}$ .

The structure factor amplitudes and phases of the  $\lambda$  phase were calculated from the structure model of  $\lambda$ - $\text{Al}_4\text{Mn}$  determined by single crystal X-ray diffraction [11]. The structure factors of  $\mu'$  were derived from those of the  $\lambda$  phase, using the strong reflections approach, as discussed below. 3D density maps of  $\mu'$  were calculated from those structure factor amplitudes and phases. Atomic coordinates were determined from the 3D density maps, using the program eMap [14]. Simulation of the electron diffraction patterns was done using the commercial CERIOUS<sup>2</sup> package (Molecular Simulations Inc., MA, USA).

## 3. Results

### 3.1. Relations between the $\mu$ , $\mu'$ and $\lambda$ phases

The  $\mu'$ - $(\text{Al,Si})_4\text{Cr}$  phase often coexists with  $\mu$ - $(\text{Al,Si})_4\text{Cr}$  and also with  $\lambda$ - $(\text{Al,Si})_4\text{Cr}$ . The three phases have well-defined orientation relationship and the strong reflections are distributed in similar positions in reciprocal space (Fig. 1). The  $hk0$  diffraction spots in  $\mu$  and  $\mu'$  coincide as shown in Fig. 1a. Moreover, the  $h00$ ,  $0k0$ , and  $h-h0$  electron diffraction spots with  $h, k = 3, 5, 8$  (Fibonacci numbers) are exceptionally strong, in agreement with the presence of pseudo-fivefold symmetry along these axial directions. The  $[010]$  SAED pattern of  $\mu'$  shows a ring of 10 strong diffraction spots (Fig. 1b), confirming the presence of a pseudo-fivefold symmetry along the  $[010]$  axis.

We thought at first that it might be possible to deduce the structure model of the  $\mu'$  phase from the  $\mu$ - $\text{Al}_4\text{Mn}$  phase, because these two hexagonal phases have the same space group  $\text{P6}_3/\text{mmc}$  and similar  $a$  parameters. However, the  $c$  parameters differ:  $\mu'$  is 1.24 nm, just one-half of that of  $\mu$  phase (2.47 nm). In  $\mu'$ , a block with  $0 < z < 0.5$  (6.2 Å thick) is symmetry-related to the neighboring block with  $0.5 < z < 1$  by a  $6_3$  operation. However, in the  $\mu$  phase, the corresponding block with  $0.125 < z < 0.375$  (also 6.2 Å thick) is NOT symmetry related to the neighboring block with  $0.375 < z < 0.625$ , but with the block at  $0.625 < z < 0.875$ . Consequently, the phase relations of the symmetry-related reflections are different for the two phases. For example, the strong reflection (505) in  $\mu'$  corresponds to (5010) in  $\mu$ . According to the space group, the phases of (505) and (50 $\bar{5}$ ) in  $\mu'$  must differ by 180°, while the corresponding reflections (5010) and (50 $\bar{10}$ ) in  $\mu$  should have the same phases. As a result, the strong reflections approach cannot be applied between the  $\mu'$  and  $\mu$  phases.

### 3.2. Deducing a structure model of $\mu'$ from $\lambda$

The  $\lambda$  phase was first found in the Al–Mn system and the structure was determined by single-crystal X-ray diffraction [11]. Later, it was also found in Al–Cr–Si alloys [12].

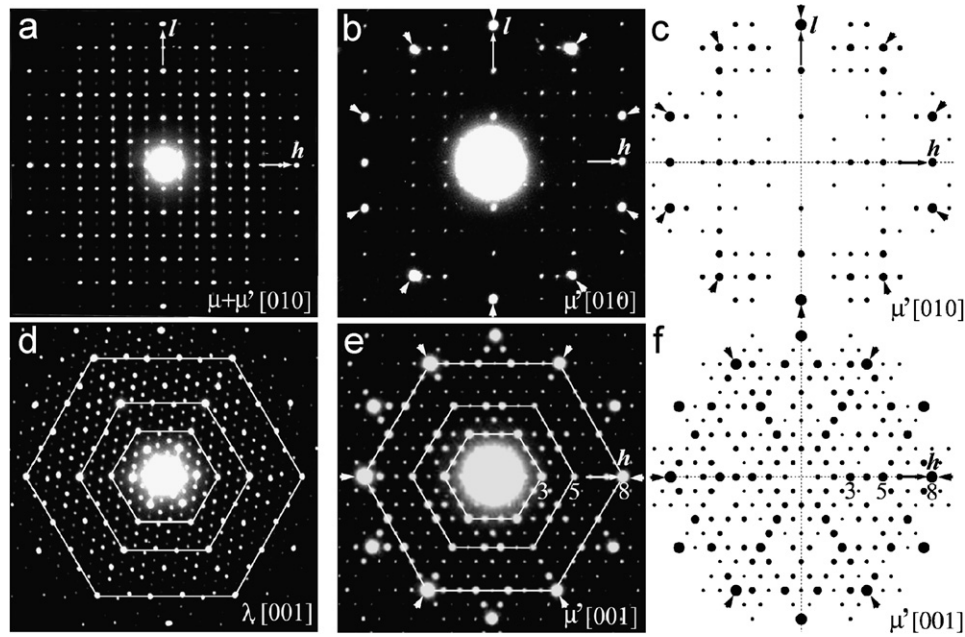


Fig. 1. Electron diffraction patterns of (a) an inter-grown area of the  $\mu$  and  $\mu'$  phases and (b) the  $\mu'$  phase taken along the  $[010]$  direction; (d) the  $\lambda$  phase and (e) the  $\mu'$  phase taken along the  $[001]$  direction, strong diffraction forming similar hexagons. (c) and (f) electron diffraction patterns of  $\mu'$  simulated from the structure model along the  $[010]$  and  $[001]$  directions, respectively.

Although the space group of the  $\lambda$  phase ( $P6_3/m$ ) is different from that of the  $\mu'$  phase, the  $c$  parameter is the same as that of the  $\mu'$  phase. The distribution of the strong reflections is also very similar for the  $\lambda$  and  $\mu'$  phases, as shown in Figs. 1d and e. The strong reflections of the  $\lambda$  phase show a higher Laue symmetry ( $6/mmm$ ) than the rest of reflections ( $6/m$ ). Remarkably, the structure factor phases of symmetry-related strong reflections of the  $\lambda$  phase obey the phase relations required for  $P6_3/mmc$ , higher than its own space group  $P6_3/m$ . This indicates that it may be possible to deduce the structure of  $\mu'$  from  $\lambda$  by the strong reflections approach, although they have different space groups. Recently, the  $\lambda$  phase was also used to deduce the structure of the hexagonal  $\tau(\mu)$  phase, with space group  $P6_3/mmc$  [4].

In order to deduce a structure model of  $\mu'$ , we have to deduce the structure factors of the strong reflections of  $\mu'$  from the corresponding structure factors of the  $\lambda$  phase. First the orientation relationship between  $\mu'$  and  $\lambda$ , defined by a matrix  $A$  as

$$(hkl)_{\mu'} = (hkl)_{\lambda} A \quad (1)$$

is determined. The matrix

$$A = \begin{pmatrix} 0.5 & 1/2\tau & 0 \\ -1/2\tau & \tau/2 & 0 \\ 0 & 0 & 1 \end{pmatrix}$$

transforms the  $hkl$  indices for  $\lambda$  into the  $hkl$  indices for  $\mu'$ . The structure factors of the  $\lambda$ - $Al_4Mn$  phase were calculated from the atomic coordinates obtained by X-ray diffraction, using the program eMap [14]. Then the 53 strongest unique

reflections in  $\lambda$  with  $F(hkl) > 500$  were selected and reindexed to the  $\mu'$  phase according to Eq. (1) and they are listed in Table 1. Five reflections falling far from the predicted position in  $\mu'$  were deleted. The structure factor phases of  $\mu'$  derived from  $\lambda$  were checked. For all the strongest reflections of  $\mu'$ , the phases of symmetry-related reflections fulfill the phase relation rules of  $P6_3/mmc$  symmetry;  $\text{Phase}(khl) = \text{Phase}(hkl) + 180^\circ$ . The 48 unique reflections of  $\lambda$  resulted in 40 unique reflections of  $\mu'$ . The new indices of the selected strongest diffraction spots are consistent with the corresponding strongest diffraction spots of  $\mu'$ . Finally, the 40 unique reflections of  $\mu'$  were expanded to a total number of 254 reflections according to the  $P6_3/mmc$  symmetry. A 3D electron density map (Fig. 2a) was calculated from the phases and the amplitudes of these reflections and the peak positions were extracted from the 3D map, using the software eMap [14]. Twenty-five unique peaks were found, two of the weakest (Nos. 22 and 25) were deleted due to short inter-atomic distances. Atom types Cr or Al/Si were assigned partly according to the peak height and partly to the previous chemical knowledge. The structure model is shown in Fig. 2b and it contains interpenetrating icosahedra chains with 3+3 or 4+2 icosahedra. The atomic coordinates and the corresponding peak heights are listed in Table 2. Note that the amplitudes used for calculating this 3D density map are not the experimental diffraction data from the  $\mu'$  phase, but those calculated from the  $\lambda$  phase. Since the amplitudes may differ somewhat for the  $\mu'$  and  $\lambda$  phases, the relative peak heights cannot be completely trusted. Thus it is not possible to assign atom types based purely on the peak heights.

Table 1  
Structure factor amplitudes and phases of the 48 strongest unique reflections in  $\lambda$  used for deriving the structure model of the  $\mu'$  phase

$h(\lambda)$	$k(\lambda)$	$l(\lambda)$	$h(\mu')$	$k(\mu')$	$l(\mu')$	$Fhkl$	Phase
0	0	6	0	0	6	3522	180
18	3	0	8	8	0	3089	0
0	0	10	0	0	10	3013	180
5	8	8	0	8	8	2864	0
5	8	2	0	8	2	2750	180
8	13	3	0	13	3	2479	180
11	2	0	5	5	0	2368	0
3	5	5	0	5	5	2287	0
10	0	3	5	3	3 <sup>a</sup>	2171	180
8	3	3	3	5	3 <sup>a</sup>	2127	0
5	8	0	0	8	0	1943	0
13	5	5	5	8	5 <sup>b</sup>	1630	180
16	0	5	8	5	5 <sup>b</sup>	1558	0
2	3	5	0	3	5	1269	180
11	2	6	5	5	6	1068	180
8	13	0	0	13	0	1064	180
3	5	4	0	5	4	952	0
0	0	8	0	0	8	937	0
0	0	2	0	0	2	933	180
5	8	4	0	8	4	927	0
10	0	0	5	3	0 <sup>c</sup>	917	180
13	5	6	5	8	6 <sup>d</sup>	898	180
16	0	6	8	5	6 <sup>d</sup>	869	180
6	10	5	0	10	5	822	180
8	3	0	3	5	0 <sup>c</sup>	761	180
11	8	2	3	10	2	754	180
0	0	4	0	0	4	749	0
2	3	6	0	3	6	715	180
8	13	2	0	13	2	670	180
8	13	4	0	13	4	639	0
3	5	9	0	5	9	626	180
3	5	1	0	5	1	598	0
10	0	9	5	3	9 <sup>e</sup>	585	0
9	4	0	3	6	0	577	0
7	11	3	0	11	3	573	0
8	3	9	3	5	9 <sup>e</sup>	566	180
8	13	1	0	13	1	564	180
10	6	5	3	8	5	557	0
13	5	3	5	8	3 <sup>f</sup>	555	0
10	0	7	5	3	7 <sup>g</sup>	546	180
5	8	6	0	8	6	540	180
10	0	2	5	3	2 <sup>h</sup>	536	180
16	0	3	8	5	3 <sup>f</sup>	529	180
8	3	7	3	5	7 <sup>g</sup>	528	0
5	8	3	0	8	3	523	0
2	3	8	0	3	8	520	180
2	3	0	0	3	0	518	0
8	3	2	3	5	2 <sup>h</sup>	515	180

<sup>abcdefgh</sup> Eight pairs of reflections (marked red) are symmetry-related in  $\mu'$ , but not in  $\lambda$ .

### 3.3. Description of the $\mu'$ structure model

There are in total 23 unique atoms in this model. According to the peaks height from the density map, and considering the chemical distributions of Al and transition metal atoms in the related  $\lambda$ , we always assigned the central atom inside an icosahedron to a transition metal atom, which has smaller atomic size than Al or Si. All the other

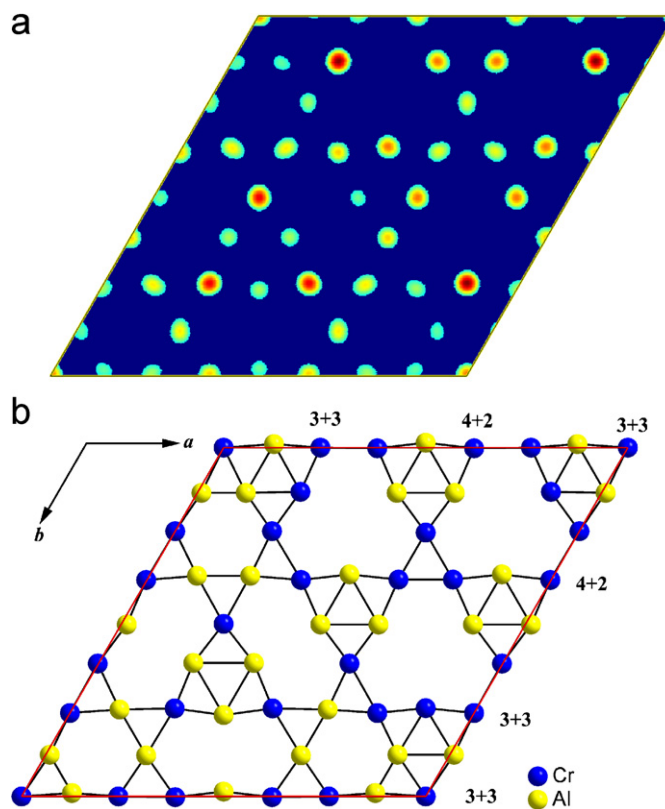


Fig. 2. The flat layer of  $\mu'$ -(Al,Si)<sub>4</sub>Cr at  $z = 0.25$  (a) the 3D density map obtained from 40 strongest unique reflections and (b) the corresponding structure model.

atom positions were assigned to be Al or Si (Al and Si are too similar to be distinguished). The final structure model for  $\mu'$  is shown in Fig. 2b, seen along the  $c$ -axis. The structure model of the  $\mu'$  phase can be described as a layer structure, with alternating flat (P) and puckered (F) atomic layers perpendicular to the  $c$ -axis. There are six layers stacked along the  $c$ -axis in each unit cell. Only two of these six layers are unique, one flat layer occurring twice (at the mirror planes  $z = 0.25$  and  $0.75$ ) and one puckered layer occurring four times (at  $z \approx 0.08, 0.42, 0.58$  and  $0.92$ ). The puckered layers located at about  $z \approx 0.08$  and  $0.42$ , and those at  $z \approx 0.58$  and  $0.92$  are related to each other by the mirror planes at  $z = 0.25$  and  $0.75$ , respectively.

The structure of  $\mu'$  can be described as interpenetrating icosahedra forming chains along the  $\langle 100 \rangle$  directions. The section corresponding to the flat layer ( $z = 0.25$ ) is shown in Fig. 3. There are 4+2 and 3+3 chains of interpenetrating icosahedra along  $\langle 100 \rangle$  directions. Six interpenetrated icosahedra (2+4 or 3+3) in  $\mu'$  compared with a chain of 10 interpenetrated icosahedra (4+4+2 or 4+3+3) in  $\tau(\mu)$  [4]. Obviously, 10/6 or 5/3 is a ratio of two successive Fibonacci numbers or an approximant of  $\tau$ . This is consistent with the  $\tau$  ratio of  $a$  parameters of  $\tau(\mu)$  and  $\mu'$ . These interpenetrating icosahedral chains are very similar to those (at  $z = 0.25$ ) in  $\mu$ -Al<sub>4</sub>Mn [6]. They form a network of icosahedra in the (001) PFP layer block. In the flat

layers, there are 9-atom truncated triangles and also 8-atom elongated hexagons around the triad axes (Fig. 4a), which are similar with the flat layer of  $\mu$ -Al<sub>4</sub>Mn at  $z = 0.75$  (Fig. 4b). Several atoms around the hexagonal axis are disordered. This is also similar to those atoms around the hexagonal axis at the puckered layer centered at about  $z = 0.325$  and the flat layer centered at  $z = 0.25$  in the structure of  $\mu$ -Al<sub>4</sub>Mn [6]. The other flat layer of  $\mu$ -Al<sub>4</sub>Mn at  $z = 0.5$  (Fig. 4c), however, is different from the flat layer at  $z = 0.75$  and  $0.25$  for  $\mu'$ .

Table 2  
Atomic coordinates of the  $\mu'$ -(Al,Si)<sub>4</sub>Cr and the corresponding peak heights on the 3D density map

Atom	<i>x</i>	<i>y</i>	<i>Z</i>	Peak height
Cr1	0.253	0.127	0.250	756
Cr2	0.252	0.505	0.250	664
Cr3	0.667	0.333	0.069	613
Al4	0.493	0.363	0.250	545
Cr5	0.000	0.000	0.250	544
Al6	0.285	0.331	0.069	494
Cr7	0.381	0.379	0.250	467
Al8	0.127	0.253	0.135	450
Al9	0.250	0.367	0.250	440
Cr10	0.622	0.378	0.250	407
Al11	0.509	0.254	0.135	400
Al12	0.205	0.409	0.059	399
Al13	0.589	0.411	0.059	350
Al14	0.284	0.569	0.069	348
Al15	0.383	0.617	0.250	344
Cr16	0.240	0.240	0.250	338
Al17	0.365	0.489	0.132	336
Al18	0.049	0.098	0.069	321
Al19	0.493	0.507	0.250	293
Al20	0.120	0.130	0.250	282
Al21	0.206	0.174	0.056	282
Al23	0.365	0.253	0.132	252
Al24	0.445	0.413	0.056	204

The [0 1 0] and [0 0 1] SAED patterns simulated from the structure model of  $\mu'$  (Figs. 1c and f) are quite similar to the corresponding experimental SAED patterns (Figs. 1b and e), respectively. Thus the structure model is basically correct. Improvement of the structure model can be made by further structure refinement against SAED data.

#### 4. Conclusions

The electron diffraction patterns (EDPs) of the  $\mu$ - and  $\lambda$ -(Al,Si)<sub>4</sub>Cr phases are almost identical to those of their counterparts in Al–Mn or Al–Cr alloys, namely, the  $\mu$ -Al<sub>4</sub>Cr/ $\mu$ -Al<sub>4</sub>Mn and  $\lambda$ -Al<sub>4</sub>Mn phases. In addition, two new phases related to  $\mu$  have been found. One is the  $\tau(\mu)$  phase with a possible space group of  $P6_3/mmc$  and  $a = 3.23$  nm and  $c = 1.24$  nm [12]. It is called  $\tau(\mu)$ -Al<sub>66</sub>Si<sub>6</sub>Cr<sub>28</sub> phase to show its  $a$  parameter being about  $\tau = (1 + \sqrt{5})/2 \cong 1.61803$  times greater than that of  $\mu$  [12].

A structure model of the new hexagonal phase  $\mu'$ -Al<sub>71.9</sub>Cr<sub>20.0</sub>Si<sub>8.1</sub> or  $\mu'$ -(Al,Si)<sub>4</sub>Cr with  $a = 2.01$  and  $c = 1.24$  nm was deduced from the known structure of the hexagonal  $\lambda$ -Al<sub>4</sub>Mn phase by the strong reflections approach. The structure consists of chains of 4+2 and 3+3 interpenetrating icosahedra running along the  $\langle 100 \rangle$  directions, which can be also found in the  $\mu$ -Al<sub>4</sub>Mn phase. There are six layers stacked along the  $c$ -axis in each unit cell for the  $\mu'$  phase while 12 layers for the  $\mu$  phase. The simulated diffraction patterns of  $\mu'$  agree with the experimental ones.

#### Acknowledgements

We thank Dr. H. Zhang for valuable discussions. This project was supported by a grant (No. 10074073) from the National Natural Science Foundation of China and the

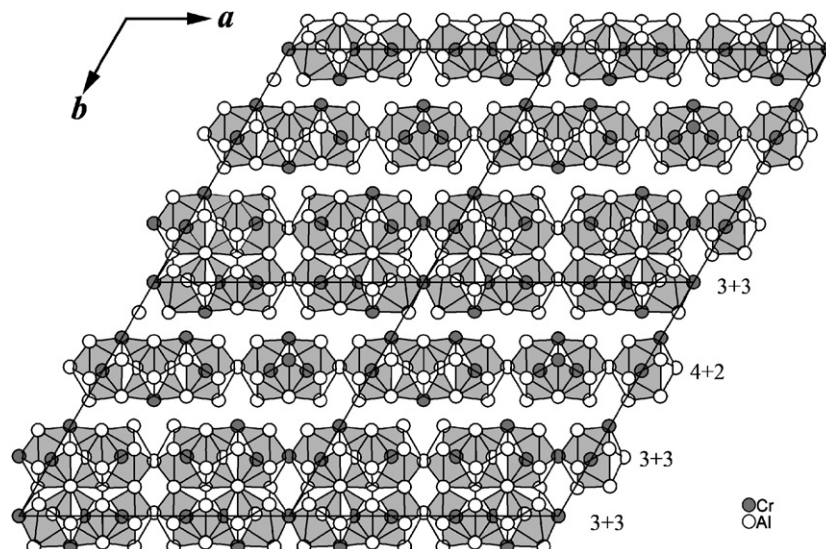


Fig. 3. The interpenetrating icosahedral chains of  $\mu'$  at  $z = 0.25$ .

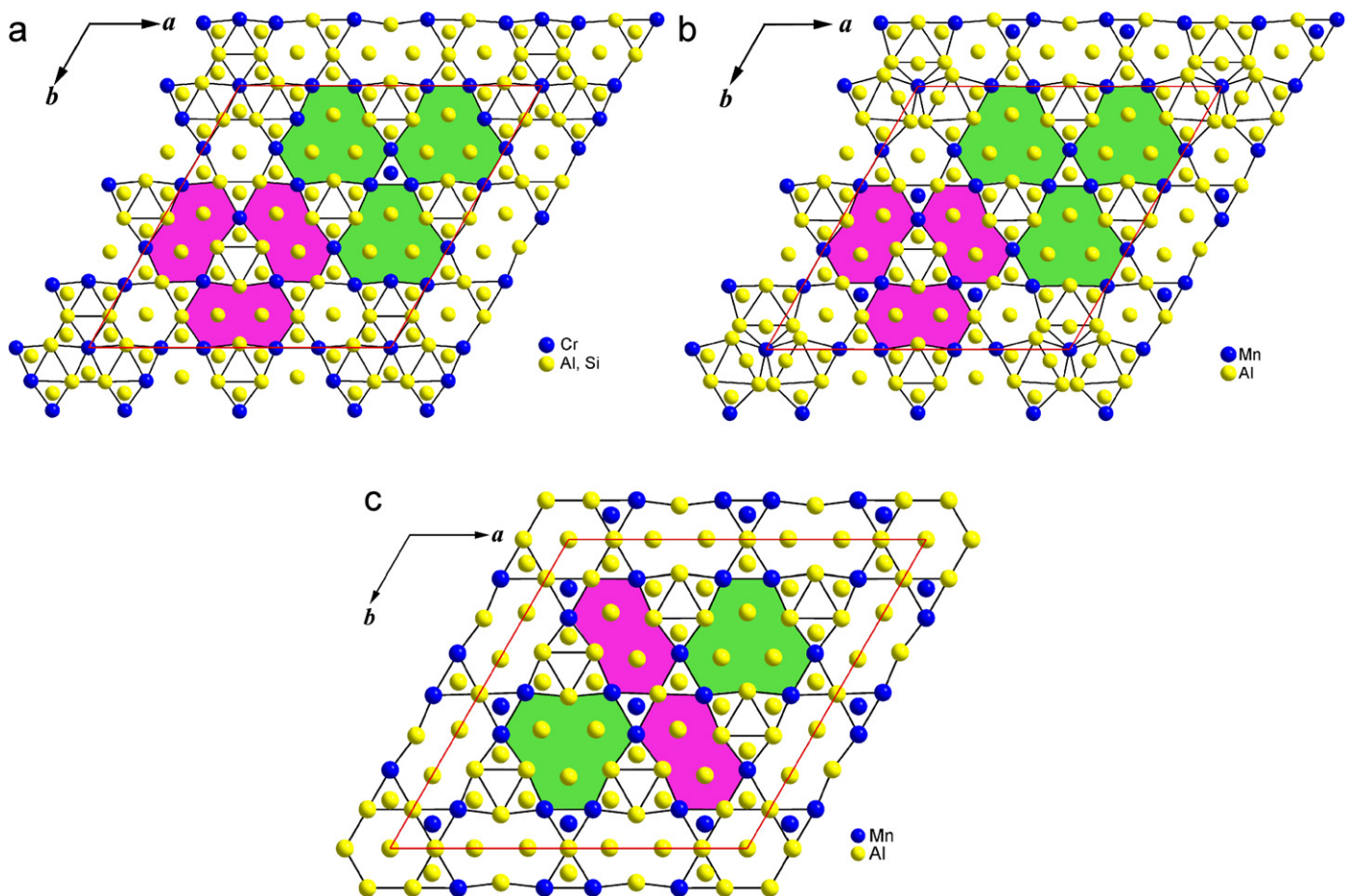


Fig. 4. A comparison of the PFP block of (a)  $\mu'$  at  $z = 0.25$ , (b)  $\mu$  at  $z = 0.75$  and (c)  $\mu$  at  $z = 0.5$ . The layer shown in (c) has no correspondence in  $\mu'$ —hence its shorter  $c$ -axis. Atoms in the flat layers are connected by thin lines. 9-atom truncated triangles and also 8-atom elongated hexagons are highlighted by green and pink areas, respectively.

Swedish Research Council. X.D. Zou is a research fellow of the Royal Swedish Academy of Sciences supported by a grant from the Knut and Alice Wallenberg Foundation.

## References

- [1] D. Shechtman, I. Blech, D. Gratias, J.W. Cahn, *Phys. Rev. Lett.* 53 (1984) 1951.
- [2] X.D. Zou, Z.M. Mo, S. Hovmöller, X.Z. Li, K.H. Kuo, *Acta Crystallogr. A* 59 (2003) 526.
- [3] H. Zhang, X.D. Zou, P. Oleynikov, S. Hovmöller, *Philos. Mag. B* 86 (2005) 543.
- [4] H. Zhang, Z.B. He, P. Oleynikov, X.D. Zou, S. Hovmöller, K.H. Kuo, *Acta Crystallogr. B* 62 (2006) 16.
- [5] Z.B. He, K.H. Kuo, *J. Alloys Compds.* 424 (2006) 164.
- [6] C.B. Shoemaker, D.A. Keszler, D.P. Shoemaker, *Acta Crystallogr. B* 45 (1989) 13.
- [7] K.Y. Wen, Y.L. Chen, K.H. Kuo, in: K.H. Kuo, T. Ninomiya (Eds.), *Quasicrystals*, World Scientific, Singapore, 1991, p. 134.
- [8] K.Y. Wen, Y.L. Chen, K.H. Kuo, *Metall. Trans. A* 23 (1992) 2437.
- [9] L.A. Bendersky, R.S. Roth, J.T. Ramon, D. Shechtman, *Metall. Trans. A* 22 (1991) 5.
- [10] M. Audier, M. Durand-Charre, E. Laclau, H. Klein, *J. Alloys Compds.* 220 (1995) 225.
- [11] G. Kreiner, H.F. Franzen, *J. Alloys Compds.* 202 (1993) L21; G. Kreiner, H.F. Franzen, *J. Alloys Compds.* 261 (1997) 83.
- [12] Z.B. He, K.H. Kuo, *J. Alloys Compds.* 373 (2004) 39.
- [13] J. Christensen, P. Oleynikov, S. Hovmöller, X.D. Zou, *Ferroelectrics* 305 (2004) 273.
- [14] P. Oleynikov, eMap, a program for generating 3D Fourier maps and determining peak positions. *AnaliTEX* [www.analitex.com/eMap.html](http://www.analitex.com/eMap.html).